Desalination and Water Treatment
www.deswater.com

doi: 10.5004/dwt.2021.26708

213 (2021) 288–302
February

Trihalomethanes (THMs) removal from aqueous solutions using environmental friendly and effective adsorbent onto *Mespilus germanica* modified by $Fe_2(MoO_4)_3$ nanocomposite on equilibrium, thermodynamic, and kinetics

Moslem Rahmani Piani[a], Maryam Abrishamkar[b,*], Bijan Mombeni Goodajdar[a], Mina Hossieni[a]

[a]*Department of Chemistry, Omidiyeh Branch, Islamic Azad University, Omidiyeh, Iran, emails: Moslemr3@gmail.com (M.R. Piani), bmombini@gmail.com (B.M. Goodajdar), Mina.hosseiny@gmail.com (M. Hossieni)*
[b]*Department of Chemistry, Ahvaz Branch, Islamic Azad University, Ahvaz, Iran, email: abrishamkarMaryam@gmail.com*

Received 30 March 2020; Accepted 20 October 2020

ABSTRACT

In the present study, the applicability of *Mespilus germanica* modified by $Fe_2(MoO_4)_3$ nanocomposite in trihalomethanes (THMs) removal from aqueous solutions has been delineated. Numerous techniques including Brunauer–Emmett–Teller, Fourier transform infrared, X-ray diffraction, and scanning electron microscopy were employed to show the characteristics of this novel material. Via employment of a batch adsorption technique, the impact values of 30 mg L^{-1}, 50 mg, 7.0, 50 min were considered as the ideal values for THMs, adsorbent mass, pH value, and contact time, respectively. Equilibrium data obtained have been to the adsorption isotherms, Langmuir, and Freundlich model best fits the experimental results. Kinetic modeling of showed that the pseudo-second-order equation was most appropriate for the description of THMs adsorption by sorbent nanocomposite. The maximum adsorption capacities for $CHCl_3$, $CHCl_2Br$, $CHClBr_2$, and $CHBr_3$ were found to be 28.5, 15.3, 13.15, and 4.27 mg g^{-1}, respectively. The thermodynamic parameters including enthalpy, entropy, and Gibbs energy were calculated for the adsorption. The negative value of ($\Delta G°$, $\Delta H°$, and $\Delta S°$) confirmed the sorption process was exothermic reflects the affinity of *M. germanica* modified by $Fe_2(MoO_4)_3$ nanocomposite for removal THMs process requires heat from aqueous solutions.

Keywords: Adsorption; Trihalomethanes; *Mespilus germanica* modified by $Fe_2(MoO_4)_3$ nanocomposite; Kinetic; Thermodynamic

1. Introduction

Disinfection is a process in which infective organisms or pathogenic micro-organisms are removed or deactivated. Water disinfection is performed before its distribution to make drinking water supplies safe and free of pathogens. For a long period, extensive use of chlorine as a disinfectant has been confirmed. However, the most important problem caused by such substances is their contribution as a precursor to the production of disinfection by-products (DBP). For this reason, more disinfectant is used in the process, so that the risk of the formation of DBP increases despite increased disinfection efficiency. Trihalomethanes (THMs) are among the most important by-products of chlorine disinfection. They have no specific smell in water but are physiologically associated with health hazards such as gene mutation and cancer [1,2]. Innumerable epidemiological investigations have reported the carcinogenicity of drinking chlorinated water in humans and animals. They have even been reported to cause increased risks of cancers for those who are exposed to chlorinated drinking water. The hazardous THMs as chlorine disinfection byproducts

* Corresponding author.

are noxious, carcinogenic, and mutagenic. Bladder, kidney, and intestine cancers are associated with THMs consumption [3–5] and the commonest forms include chloroform ($CHCl_3$), dichlorobromo methane ($CHBrCl_2$), dibromochloro methane ($CHBr_2Cl$), and bromoform ($CHBr_3$). Many studies have reported the incidence of cancer in laboratory animals which were exposed to chloroform as an indicator of THMs. Moreover, some researchers have found a relationship between these compounds and stillbirth [6], coagulation and ion exchange [7], adsorption [8], ozonation and air oxidation [9], nanofiltration [10], GAC and air stripping columns [11], and biosorption [12] are among the conventional wastewater treatment protocols based on physicochemical, chemical, and biological processes. Adsorption application outstripped others in large scale chemical, biochemical, environmental recovery, and purification applications [13]. The popularity of this technique is due to the advantages of (1) simple design, (2) simple operation, (3) being efficient, (4) application of non-toxic and inexpensive adsorbents. The appropriateness of adsorbents is confirmed based on their properties and characteristics by considering factors like removal capacity, operating conditions, and treatment costs [14]. Therefore, the essentiality of applying more suitable methods for the elimination of THMs and their precursors is apparent. Thus, among different methods, the adsorption process is the best method in eliminating organic pollutants like THMs and humic acid owing to its efficiency and simplicity. In theory, activated carbon is considered as the most appropriate adsorbent for THMs elimination; however, on the practical level, it demonstrates the low capacity for the elimination of NOM which is a high molecular organic compound [15]. Other adsorbents such as volatile ash, bentonite, and pumice stone types of biomasses, powder activated carbon, coke, and kaolin are also used in organic pollutants' adsorption [16,17]. However, such adsorbents are expensive, so the utilization of low-cost adsorbents not only has drawn the attention of researchers but has also been synthesized and studied to check their feasibility [18].

In the last decades, several NCs have been fabricated for the adsorptive removal of heavy metals from water and wastewater. Recently, blending of the nano composite matrix with inorganic nanomaterials has occupied an impressive platform of research because of their simplicity, stable performance, and mild operating conditions [19]. This type of surface modification stabilizes the NPs against the agglomeration and also makes them compatible with the other phase. The suitable surface modification of NPs, not only leads to enhanced dispersion and compatibility in composite matrix, but also undergoes chemical or physical interactions with the composite matrix. The conventional wastewater treatment protocol is usually based on physicochemical, chemical, and biological processes. Amongst the mentioned processes, adsorption is extensively employed for large scale chemical, biochemical, purification, and environmental recovery applications [20]. Using effective, non-toxic, and low-cost adsorbents along with simple its design and ease of operation has made this technique beneficial and popular. Appropriateness of the adsorbent depends on factors such as elimination capacity, treatment costs, and operating conditions.

The application of chemical treatment and the biodegradation procedure are unpopular since they are costly and complex processes and produce hazardous byproducts. *Mespilu germanica* tree grows in many regions indicating that this activated carbon derived from *Mespilus germanica* is very inexpensive, energy saving, and the most important of all non-toxic. All these characteristics make *M. germanica* modified by $Fe_2(MoO_4)_3$ nanocomposite a potential carbon in eliminating water pollution when juxtaposed against other commercial materials. On the contrary, the use of biological treatment and chemical precipitation in eliminating THMs is eco-unfriendly and has low efficiency [21]. Additionally, in order to remove heavy metals and organic pollutants from water, many attempts have been made to produce useful adsorbents with various chemical compounds and superficial properties [22].

Thus, preparing activated carbon derived from *M. germanica* modified by $Fe_2(MoO_4)_3$ nanocomposite was carried out and used as an alternative to exorbitant or hazardous adsorbents for the elimination of THMs from wastewater. To characterize the *M. germanica* modified by $Fe_2(MoO_4)_3$ nanocomposite, its X-ray diffraction (XRD) pattern and Fourier transform infrared (FTIR) were applied. Accordingly, a thorough examination was performed on the experimental conditions of contact time, the pH of the solution, and adsorbent dosage and the removal percentage of THMs as a response was performed and the values were optimized. The boundaries of interaction between experimental factors came under scrutiny. PH of 7, the contact time of 50 min, initial THMs concentration of 30 mg L^{-1}, and adsorbent dosage of 50 mg were determined as the optimal conditions for the elimination of THMs. Varied isotherm models, namely Freundlich, Langmuir, Temkin, and Dubinin–Radushkevich were applied to fit the experimental equilibrium data. The fitness and relevance of the Dubinin–Radushkevich model was proven by the obtained outcomes. Considering the kinetic models of pseudo-first-order, the pseudo-second-order, and Elovich diffusion models confirmed the dominance of the pseudo-second-order model in the kinetic of adsorption process. The *M. germanica* modified by $Fe_2(MoO_4)_3$ nanocomposite proved to be effective in eliminating the THMs from wastewater.

2. Materials and methods

2.1. Preparation of stock solution

All used chemicals were of reagent grade and utilized without further purification. For the pH adjustment, HCl (hydrochloric acid), and NaOH (sodium hydroxide) were applied. The preparation of THM solutions was done synthetically by diluting 2,000 mg L^{-1} analytical grade THM solution (SupelcoInc., Bellefonte, USA). Also, to attain the desired THMs concentration, equivalent concentrations of $CHCl_3$, $CHCl_2Br$, $CHClBr_2$, and $CHBr_3$ were added into deionized water [8].

2.2. Instrumentation

UV-vis spectrophotometer (Jasco, model UV-vis V-530, Japan). FTIR spectra were recorded on a PerkinElmer (FT-IR spectrum BX, Germany). The morphology of samples was studied by scanning electron microscopy (SEM: KYKY-EM

3200, Hitachi Company, China) under an acceleration voltage of 26 kV. Transmission electron microscopy (TEM) images were taken on a JEOL 3010. The pH/ion meter (model-728, Metrohm Company, Switzerland, Swiss) was used for the pH measurements. Laboratory glassware was kept overnight in 10% nitric acid solution.

2.3. Preparation of the M. germanica

The following steps show the preparation of *M. germanica*: first, the leaves of the *M. germanica* were picked. Second, they were washed completely with plenty of water and dishwashing liquid. Then, at an ambient temperature, first they were hung out to dry and then were dried at 80°C for 50 min in an oven. The carbon was dissolved by grinding and milling the carbon black, for separating and grinding with a mesh of 80–100 or 100–200. Micro-leaf particles were put in a solution of chloride and concentrated nitric acid for 12 h. Next, the carbon was cleaned and washed twice with distilled water (DW) till the pH of the water below the filter became approximate to 7. The carbons were desiccated in an oven for 24 h at a temperature of about 100 and poured into the plastic container in an anti-moisture container.

2.4. Preparation of M. germanica modified by $Fe_2(MoO_4)_3$ nanocomposite

The iron oxide-molybdenum nanocomposite was prepared in a synergistic process by mixing the juice solutions of heptemolybdate ammonium and iron nitrate. Ammonium heptamolybdate ($[NH_4]_6Mo_7O_{24}\cdot 4H_2O$]) was charged into 175 mL distilled water disintegrated solution and the pH of the solution was adjusted to 1.8 with concentrated chloride. A solution containing 50 g of iron nitrate [$Fe(NO_3)_3\cdot 4H_2O$] with 350 mL of deionized distilled water was obtained. The container with the heptamol dilution of ammonium was positioned in a warm bath with a temperature of 70°C. The iron nitrate solution was added slowly while the ammonium heptamolybdate solution was being stirred. Then, the bath temperature was increased to 90°C. The sediment suspension was stirred for 3 h. Stirring was stopped and the suspension was placed in the laboratory for 2 h. The carbon was produced from a leaf medlar with an equal weight ratio and after analysis was utilized with SEM, BET, FT-IR, and XRD as an adsorbent [23].

2.5. Batch adsorption of THMs adsorption process

To ascertain the $CHCl_3$, $CHCl_2Br$, $CHClBr_2$, and $CHBr_3$ adsorption isotherm onto *M. germanica* modified by $Fe_2(MoO_4)_3$ nanocomposite and its thermodynamic properties, batch adsorption experiments were performed. The preparation of 100 mL solution with 30 mg L^{-1} concentration of $CHCl_3$, $CHCl_2Br$, $CHClBr_2$, and $CHBr_3$ was carried out and by using 0.01 N HCl/0.01 N NaOH aqueous solution. The initial pH of the solution was adjusted without any further adjustments during the experiments. In 10 flasks (100 mL) with a fixed adsorbent dose of 30 mg L^{-1}, 10 samples of 50 mL solution were provided. Then, these 10 flasks were agitated through the instrumentality of an orbital shaker at a constant rate of 200 rpm at a temperature maintained at 25°C temperatures. After fixed time intervals (10 at 80 min), one of the samples was withdrawn and analyzed for remaining THMs in the adsorbate solution. With the help of Whatman No. 42 filter paper, *M. germanica* modified by $Fe_2(MoO_4)_3$ was filtered from the aqueous solution. A double beam UV-vis spectrophotometer (Jasco, model UV-vis V-530, Japan) was set at wavelengths 350 nm and the $CHCl_3$, $CHCl_2Br$, $CHClBr_2$, and $CHBr_3$ concentration in the solution was measured. The calculation of the quantity of adsorbed $CHCl_3$, $CHCl_2Br$, $CHClBr_2$, and $CHBr_3$ at equilibrium (q_e (mg g^{-1})) was done applying the ensuing equation:

$$\%A = \frac{C_0 - C_e}{C_t} \times 100 \tag{1}$$

where C_0 (mg L^{-1}) in the above equation is the concentration of target at initial time t and C_t (mg L^{-1}) is that after time t.

$$q_e = \frac{(C_0 - C_e)V}{W} \tag{2}$$

where C_0 (mg L^{-1}) is the initial THMs concentration and C_e (mg L^{-1}) refers to equilibrium THMs concentration in aqueous solution in the solution volume and the adsorbent mass are shown by V (L) and W (g), respectively. The evaluation of the thermodynamic properties of the adsorption process was performed by adding 50 mg of *M. germanica* modified by $Fe_2(MoO_4)_3$ nanocomposite into 100 mL initial $CHCl_3$, $CHCl_2Br$, $CHClBr_2$, and $CHBr_3$ concentration ranging from 10 to 60 mg L^{-1} in each experiment. For 50 min and at 25°C, each solution was shaken uninterruptedly. The $CHCl_3$, $CHCl_2Br$, $CHClBr_2$, and $CHBr_3$ concentrations were estimated after the solution equilibrium and the desorption outcomes were obtained.

2.6. Adsorption mechanism of THMs

The physical and chemical characteristics of *M. germanica* Modified by $Fe_2(MoO_4)_3$ nanocomposite were substantially changed by calcination. The specific surface area and the amount of polar functional groups increased, and the adsorption performance improved. Overall, the mechanisms of adsorption of THMs on *M. germanica* modified by $Fe_2(MoO_4)_3$ nanocomposite were mainly attributed to two aspects: chemical adsorption and physical adsorption. Under acidic conditions, chemical adsorption is dominant. The carboxyl of THMs undergoes ion and/or proton exchange reactions with the reactive sites of $Fe_2(MoO_4)_3$ NPS-AC with hydroxyl groups. Hydroxyl groups on the adsorbent combine with H^+ in solution, thus resulting in a greater hydroxyl group exchange and the formation of ($-OH_2^+$), according to Eqs. (A). Furthermore, proton exchange reactions occur between $-OH_2^+$ and the hydroxyl group with outer complexes (Eqs. (B)). Finally, the inner complex is formed by ligand exchange, according to Eqs. (C).

$$Fe_2(MoO_4)_3\ \text{NPS-AC} - OH + H^+ \rightarrow Fe_2(MoO_4)_3\ \text{NPS-AC} - OH_2^+ \tag{A}$$

$$Fe_2(MoO_4)_3\ NPS\text{-}AC - OH_2^+ + THM - C(O)O^- \leftrightarrow AR - OH_2^+O^- - C(O) - THM \quad (B)$$

$$Fe_2(MoO_4)_3\ NPS\text{-}AC - OH_2^+O^- - C(O) - THM \leftrightarrow Fe_2(MoO_4)_3\ NPS\text{-}AC - OC(O) - THM + H_2O \quad (C)$$

In neutral and weak alkaline conditions, THMs exhibits substantial proton loss and exist as free ions in solution, thus inhibiting the chemical adsorption to some extent. However, the porous structure of $Fe_2(MoO_4)_3$ NPS-AC, especially after modification, tempers the negative effect via physical adsorption [24].

3. Results and discussion

3.1. Characterization of adsorbent

Bulk density, surface area, and loss of mass on ignition are shown in Table 1. The bulk density affects the rate of adsorption of THMs solution *M. germanica* modified by $Fe_2(MoO_4)_3$ nanocomposite. In the present study, the bulk density was less than 1.0 indicating that the activated carbon materials are in fine nature and hence enhanced the adsorption of THMs solution from aqueous solution [25]. The moisture content (0.5%) was determined, even though it does not affect the adsorption power, dilutes the adsorbents, and therefore necessitates the use of additional weight of adsorbents to provide the required weight. The surface area of *M. germanica* modified by $Fe_2(MoO_4)_3$ nanocomposite in the present research study was 250 $m^2\ g^{-1}$ and is higher than a low cost agro-based adsorbent such as *M. germanica* modified by $Fe_2(MoO_4)_3$ nanocomposite (45.231 $m^2\ g^{-1}$ and $1.34 \times 10^{-2}\ cm^3\ g^{-1}$) (Fig. 1).

3.2. Characterization of adsorbent

Fig. 2 demonstrates the FTIR spectrum of *M. germanica* modified by $Fe_2(MoO_4)_3$ nanocomposite. While the broad signals at 1,231–1,441 cm^{-1} is ascribable to C–H stretching from phenolic and alcoholic groups, the one at 1,640 cm^{-1} is attributable to C=O bonds. Also the apparent signals at 2,917 and 3,422 cm^{-1} are attributable to C–OH stretching [26]. The energy-dispersive X-ray spectroscopy (EDX) spectrum of *M. Germanica* is exhibited in Fig. 3a. It is worth noting that, after surface modification with $Fe_2(MoO_4)_3$, functionalized *M. germanica* became uneven. In Fig. 3b, the EDX spectrum of *M. germanica* modified by $Fe_2(MoO_4)_3$ nanocomposite is shown [27].

3.3. XRD analysis

Visible signals in the XRD pattern of the *M. germanica* modified by $Fe_2(MoO_4)_3$ nanocomposite (Fig. 5b) at 62.0(440), 56.0(511), 44.75(400), 37.2(311), 33.0(220), and 21.45(111) are related to diffractions and reflections from the carbon atoms *M. germanica*. As one can see, after functionalizing with $Fe_2(MoO_4)_3$, the extremely crystalline nature of the material is revealed while the great intensity of the signal at 37.2(311) proves that a small quantity of the material is noncrystalline. The proper synthesis of the developed *M. germanica* modified by $Fe_2(MoO_4)_3$ nanocomposite is confirmed by the XRD patterns. Fig. 4, represents the Raman pattern of the *M. germanica* and *M. germanica* modified by $Fe_2(MoO_4)_3$ nanocomposite [28].

3.4. Surface morphology M. germanica modified by $Fe_2(MoO_4)_3$ nanocomposite

The graph in Fig. 5 shows the morphological features and particle size distribution of the *M. germanica* modified

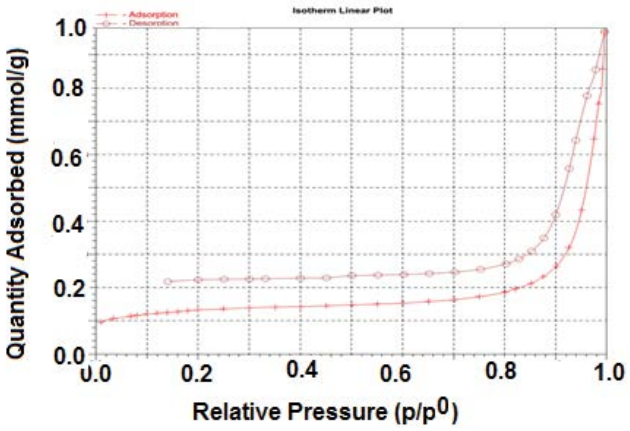

Fig. 1. Physisorption isotherm of *Mespilus germanica* modified by $Fe_2(MoO_4)_3$ nanocomposite.

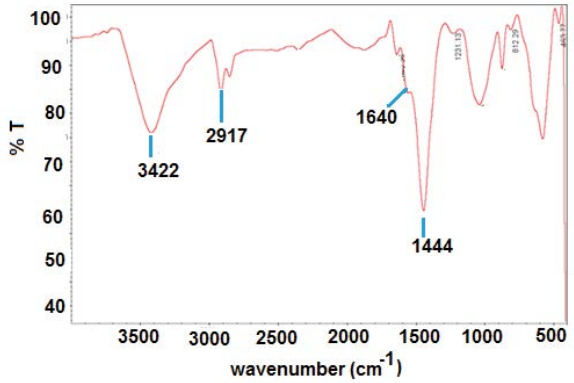

Fig. 2. FT-IR of the developed *Mespilus germanica* modified by $Fe_2(MoO_4)_3$.

Table 1
Characteristics of the *Mespilus germanica* modified by $Fe_2(MoO_4)_3$ nanocomposite

Parameter	pH	Moisture (%)	Bulk density ($g\ L^{-1}$)	Surface area ($m^2\ g^{-1}$)	Particle size range (μm)	Loss of mass on ignition
Value	7.0	0.5	0.45	250	45–250	0.6235

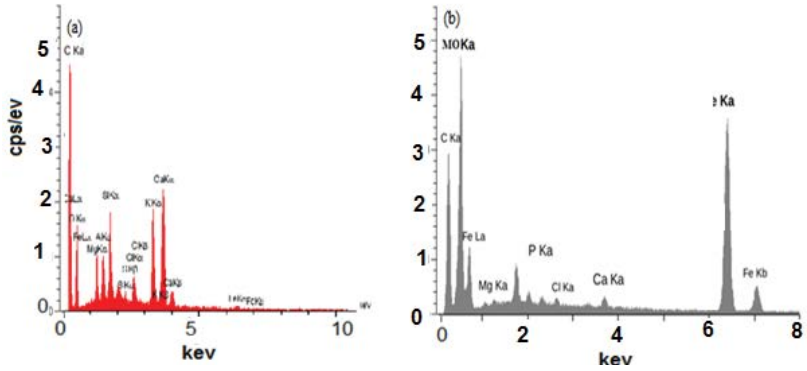

Fig. 3. (a) Energy-dispersive X-ray spectroscopy (EDX) spectrum of *Mespilus germanica* and (b) EDX transmittance spectrum of the prepared *Mespilus germanica* modified by $Fe_2(MoO_4)_3$ nanocomposite.

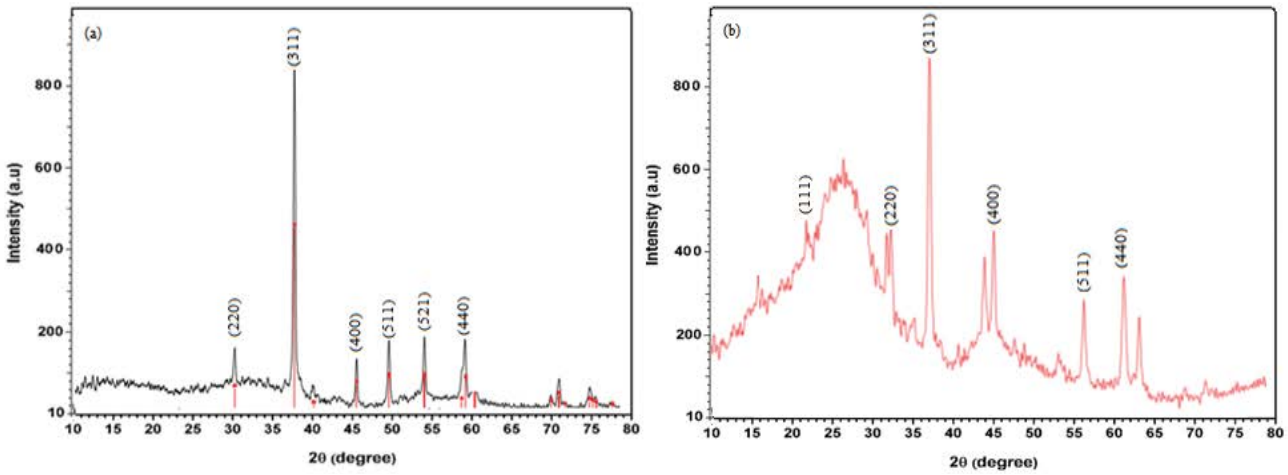

Fig. 4. (a) XRD of the prepared *Mespilus germanica* and (b) XRD of the prepared *Mespilus germanica* modified by $Fe_2(MoO_4)_3$ nanocomposite.

by $Fe_2(MoO_4)_3$ nanocomposite using the SEM micrograph. It has been seen that the particles were mostly spherical with various size distribution as they form agglomerates. From the particle size distribution, we obtain the average particle size in the range of 44–57 nm, very close to those determined by XRD analysis [29].

3.5. Raman spectroscopy

Raman scattering is a tool to study the behavior of the atomic clusters, scattering of light in the shortrange order probe as well as nanostructure materials. It is well-known that in semiconductors, the observed Raman shifts usually correspond to the longitudinal optical (LO) phonons (LO), whereas other modes such as the transverse optic (TO) and the surface phonon (SP) modes in general are not observable because of symmetry restrictions and low intensities. However, as the surface to volume ratio is large in the case of nanostructure materials, it is possible to observe SP mode by Raman scattering measurements [30]. The Raman scattering is sensitive to small disorders, even at regions as small as few unit cells. Fig. 6 shows the Raman spectra of *M. germanica* modified by $Fe_2(MoO_4)_3$ nanocomposite thin films deposited at different substrate temperatures.

3.6. Impact of pH on the adsorption of THMs

The role of the pH value in the adsorption process is of significant importance. In Fig. 7, the elimination of THMs as a function of pH at diverse sorbents is displayed. To determine the desired pH for the perfect elimination of THMs at diverse pH levels from 2.0 to 9.0, the measurement of equilibrium adsorption of THMs was performed by adjusting the initial THMs concentrations at 30 ppm. Table 2 displays the results in summary [31]. The perfect removal percentages of THMs at pH = 7.0 as a desired pH was for pure $CHCl_3$, $CHCl_2Br$, $CHClBr_2$, and $CHBr_3$ at roughly 87.4%, 84.2%, 80.9%, and 78.3%, respectively. A sharp decrease in THMs removal was observed at pH < 7 which is due to the competition of THMs with H^+. Also, the high concentration of H^+. Also, in very acidic pH can lead to protonation of nitrogen atoms on the surface of adsorbents and provoke reduction of interaction between THMs and surface adsorbents. Abatement in the elimination of THMs at alkaline pH (>7) is due to the precipitation of hydroxide and also the conversion of THMs. Therefore, this phenomenon is a major impediment for THMs molecules to have access to adsorption sites which brings about less adsorption of THMs [32].

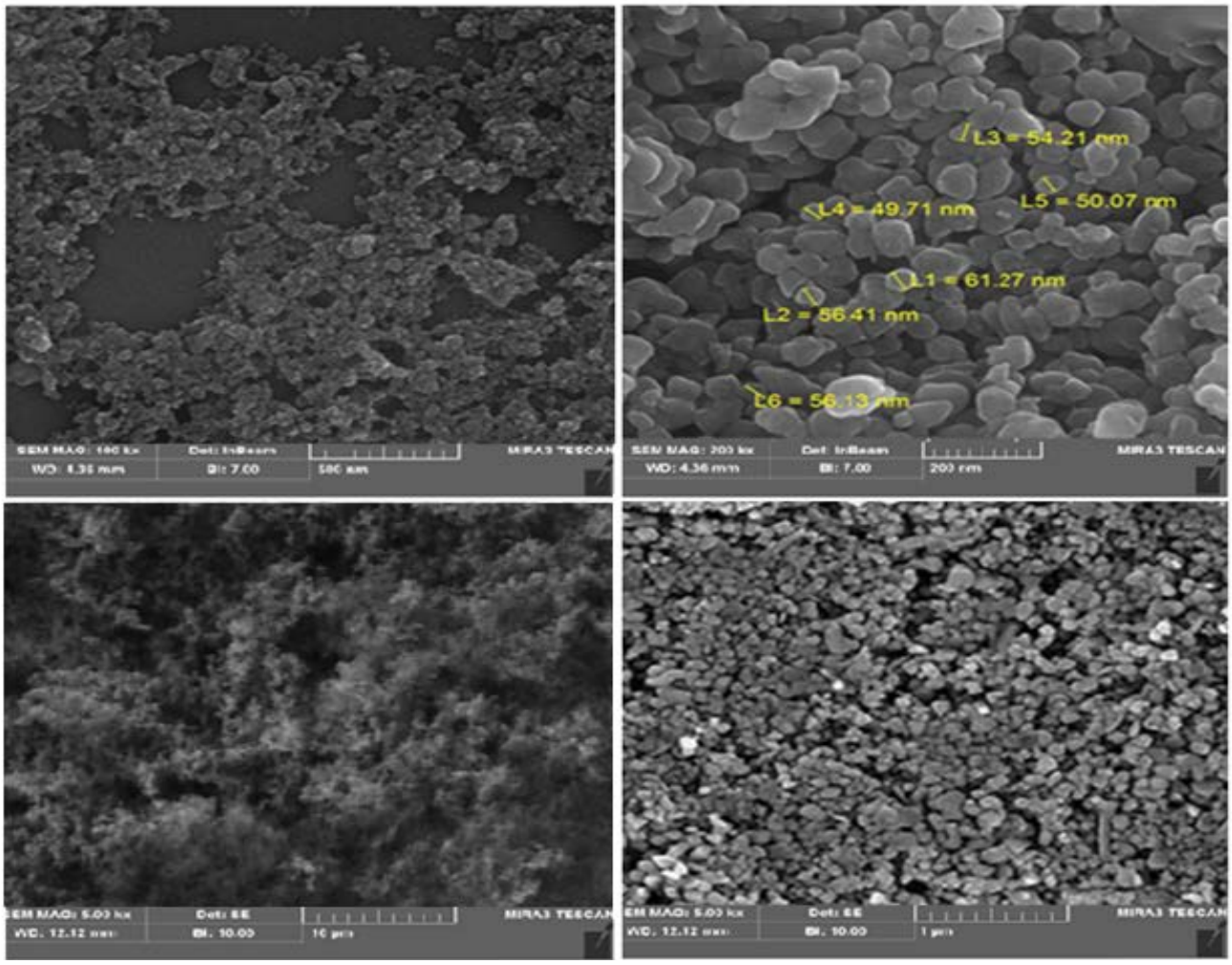

Fig. 5. SEM image of the prepared *Mespilus germanica* modified by $Fe_2(MoO_4)_3$ nanocomposite.

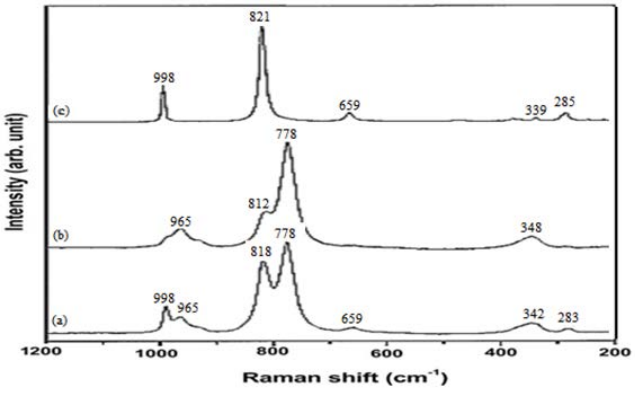

Fig. 6. Raman of the prepared (a) $(MoO)_3/Fe_2(MoO_4)_3$, (b) $Fe_2(MoO_4)_3$, and (c) $(MoO)_3$.

3.7. Impact of initial THMs concentration

Investigation about the adsorption uptake of THMs was done for initial concentration range from 10 to 60 mg L^{-1} and exhibited in Fig. 8. The essential features of a Langmuir isotherm can be expressed in terms of a dimensionless constant separation factor or equilibrium parameter, R_L that is used to predict if an adsorption system is favorable or unfavorable. The essential characteristic separation constant factor, R_L, for the Langmuir adsorption is defined as follows:

$$R_L = \frac{1}{1 + K_L C_0} \tag{3}$$

The value of R_L illustrates the shape of the isotherm to be either unfavorable ($R_L > 1$), linear ($R_L = 1$), favorable ($0 < R_L < 1$), or irreversible ($R_L = 0$). The calculated R_L values vs. initial of $CHCl_3$, $CHCl_2Br$, $CHClBr_2$, and $CHBr_3$ concentration are given in Fig. 8, indicating that the Langmuir adsorption of $CHCl_3$, $CHCl_2Br$, $CHClBr_2$, and $CHBr_3$ onto *M. germanica* modified by $Fe_2(MoO_4)_3$ nanocomposite is favorable.

A rise in the initial concentration of THMs provokes the increase in the adsorption yield of $CHCl_3$, $CHCl_2Br$, $CHClBr_2$, and $CHBr_3$ by *M. germanica* modified by $Fe_2(MoO_4)_3$ nanocomposite. The requisite driving force is provided by the initial concentration to defeat the resistance to mass transfer of adsorbent between aqueous and solid phases [33].

3.8. Impact of the dosage of adsorbents

Through changing the adsorbents dosage in the range of 10–70 mg, the net result of biosorbents dosage on percentage removal of THMs was examined. Based on what is observed in Fig. 9, the percentage removal of THMs boosted when the adsorbent dosage increased. Biosorbents dosage of 50 mg and constant initial trihallomethans concentration of 30 mg L^{-1} were chosen as the desired values since the highest removal percentages of 88.0%, 83.3%, 78.8%, and 73.1%, were obtained for $CHCl_3$, $CHCl_2Br$, $CHClBr_2$, and $CHBr_3$ respectively at these values. The phenomenon which greater adsorbent dose is equal to greater removal percentage of THMs is explainable in this way that when adsorbent dosage increases, more and more surface becomes available for metal ion to adsorb and this will boost the rate of adsorption [34].

3.9. Impact of the contact time on the adsorption of THMs

The influence of contact time on sorption of THMs by synthesized *M. germanica* modified by $Fe_2(MoO_4)_3$ is properly exhibited in Fig. 10. A slight change in sorption rate became apparent 10 at 80 min for pure $CHCl_3$, $CHCl_2Br$, $CHClBr_2$, and $CHBr_3$, respectively. After that, this change was starting to level off gradually until no significant increase was observed in the THMs adsorption and elimination eventually reached equilibrium [35]. Therefore, at contact times of 50 min, the highest removal percentages for $CHCl_3$, $CHCl_2Br$, $CHClBr_2$, and $CHBr_3$ are 88.4%, 83.6%, 79.0%, and 73.5%, respectively.

3.10. Impact of temperature

The impact of temperature on the adsorption of THMs is demonstrated in Fig. 11. The temperatures from 298.15 to 348.15 K were selected for performing the experiments. The impact of temperature on the sorption of $CHCl_3$, $CHCl_2Br$, $CHClBr_2$, and $CHBr_3$ on *M. germanica* modified by $Fe_2(MoO_4)_3$ nanocomposite. Accordingly, the endothermicity nature of the adsorption is confirmed by aforementioned results. Thus, by considering the porosity nature of the adsorbent and the likelihood of diffusion of adsorbate, sorption will increase with the rise of temperature that affects the diffusion. In addition, as the process is endothermic, the rise in temperature works for the benefit of the adsorbate transport within the pores of adsorbent [36].

3.11. Biosorption isotherms

The subdivision of sorbate molecules that are subdivided between liquid and solid phases at equilibrium is described by adsorption isotherm. Through the instrumentality of four adsorption isotherms of Freundlich, Langmuir,

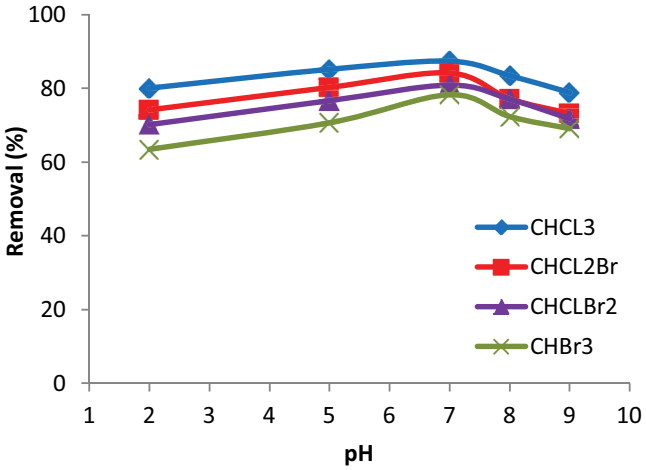

Fig. 7. Impact of pH on the elimination of THMs (THMs conc = 30 mg L^{-1}, adsorbent dose = 50 mg, contact time = 50 min, stirring speed = 180 rpm, and temperature = 25°C).

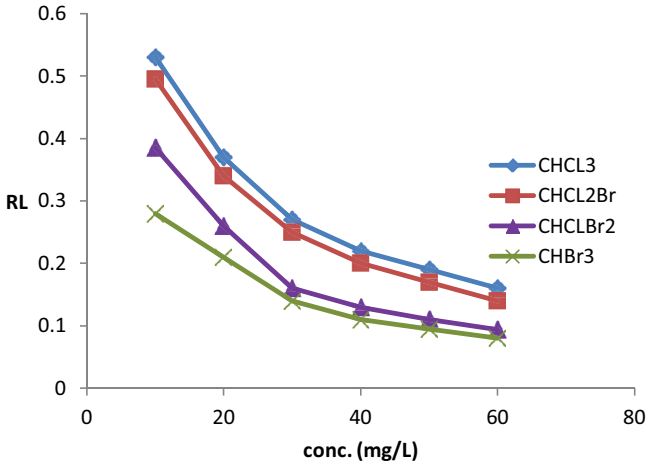

Fig. 8. Impact of initial THMs elimination (pH = 7.0, dose of adsorbent = 50 mg, contact time = 50 min, stirring speed = 180 rpm, and temperature = 25°C).

Table 2
Adsoption quality and distribution coefficient parameters for $CHCl_3$, $CHCl_2Br$, $CHClBr_2$, and $CHBr_3$ solution (30 mg L^{-1}, pH = 7), onto *Mespilus germanica* modified by $Fe_2(MoO_4)_3$ nanocomposite

Sample	THMs contact solution (mg L^{-1})		Removal efficiency (%)	k_d (mL g^{-1}) 10^3	q_e
	Initial (C_i)	Final (C_e)			
$CHBr_3$	100	21/7	78.3	3.132	6.796
$CHClBr_2$	100	19/1	80.9	3.236	6.181
$CHCl_2Br$	100	15/8	84.2	3.368	5.321
$CHCl_3$	100	12/6	87.4	3.496	4.405

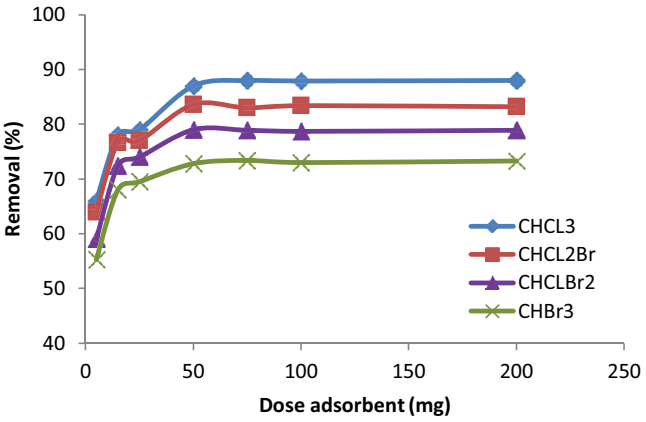

Fig. 9. Impact of adsorbent dosage on THMs elimination (THMs conc = 30 mg L^{-1}, pH = 7.0, contact time = 50 min, stirring speed = 180 rpm, and temperature = 25°C).

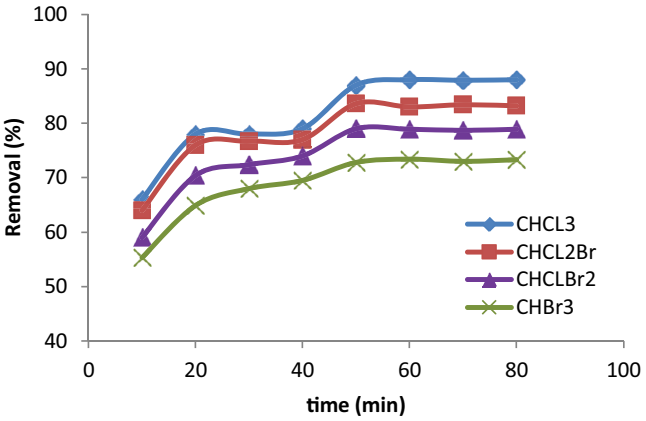

Fig. 10. Impact of time on THMs elimination (THMs conc = 30 mg L^{-1}, pH = 7.0, contact dose of adsorbent = 50 mg, stirring speed = 180 rpm, and temperature = 25°C).

Temkin, and Dubinin–Radushkevich isotherms, adsorption of $CHCl_3$, $CHCl_2Br$, $CHClBr_2$, and $CHBr_3$ onto *M. germanica* modified by $Fe_2(MoO_4)_3$ nanocomposite was modeled [37].

3.12. Adsorption equilibrium study

The equilibrium relationship based on mathematical connection of an established equilibrium between the quantity of adsorbed target per gram of adsorbent (q_e (mg g^{-1})) and the equilibrium non-adsorbed quantity of ions in solution (C_e (mg L^{-1}) at specified temperature is defined by adsorption equilibrium isotherms [38]. The adsorption isotherm of adsorption was evaluated by using four models of Freundlich adsorption isotherm, Langmuir adsorption isotherm, Temkin adsorption isotherm, and Dubinin–Radushkevich (D–R) isotherms.

- In Langmuir adsorption isotherm, no interaction occurred amongst adsorbed molecules and the adsorption process on uniform surfaces. The ensuing equation presents the Langmuir model clearly [39]:

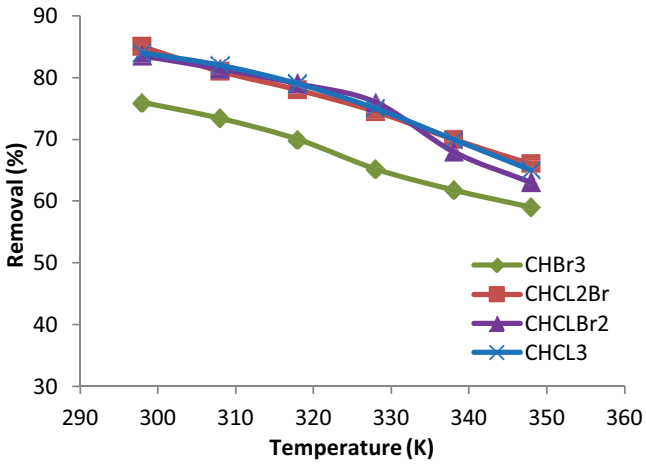

Fig. 11. Impact of temperature on THMs elimination (THMs conc = 30 mg L^{-1}, dose of adsorbent = 50 mg, pH = 7.0, contact time = 50 min, and stirring speed = 180 rpm).

$$\frac{C_e}{q_e} = \frac{1}{K_L q_{\max}} + \frac{C_e}{q_{\max}} \tag{4}$$

In the aforementioned equation, the equilibrium concentration, the adsorption capacity and the maximum adsorption capacity of the adsorbents in the aqueous medium are shown by C_e (mg L^{-1}), q_e (mg g^{-1}), and $q_{\max}$ (mg g^{-1}) respectively. K_L as a constant is relative to binding energy of the sorption system (L mg^{-1}) (Fig. 12a).

- Freundlich adsorption isotherm explains the multilayer adsorption of an adsorbate onto a non-uniform surface of an adsorbent. The following introduces the linear form of Freundlich isotherm model:

$$\log q_e = \log K_f + \frac{1}{n}\log C_e \tag{5}$$

The Freundlich isotherm constants are the K_F (the adsorption capacity) and n (intensity of a given adsorbent) (Fig. 12b).

For the both models, the slope and the position of the constant determined their values (Figs. 12a and b). The outcomes of the fit and of the constants of both models for four $CHCl_3$, $CHCl_2Br$, $CHClBr_2$, and $CHBr_3$ are shown in Table 3. The values of n for $CHCl_3$, $CHCl_2Br$, $CHClBr_2$, and $CHBr_3$ were 0.42, 0.30, 0.28, and 0.16, respectively. The desired value for n in the adsorption process was between 1 and 10 [40]. The Langmuir isotherm was confirmed to be the perfect model to demonstrate the adsorption of $CHCl_3$, $CHCl_2Br$, $CHClBr_2$, and $CHBr_3$ onto *M. germanica* modified by $Fe_2(MoO_4)_3$ nanocomposite adsorbent based on all the correlation coefficients and parameters obtained for the isotherm models (Table 3).

- There is a presumption in Temkin isotherm equation that the heat of biosorption of all the molecules in the layer abates linearly with coverage because of adsorbent–adsorbate interactions. It is also presumed that the

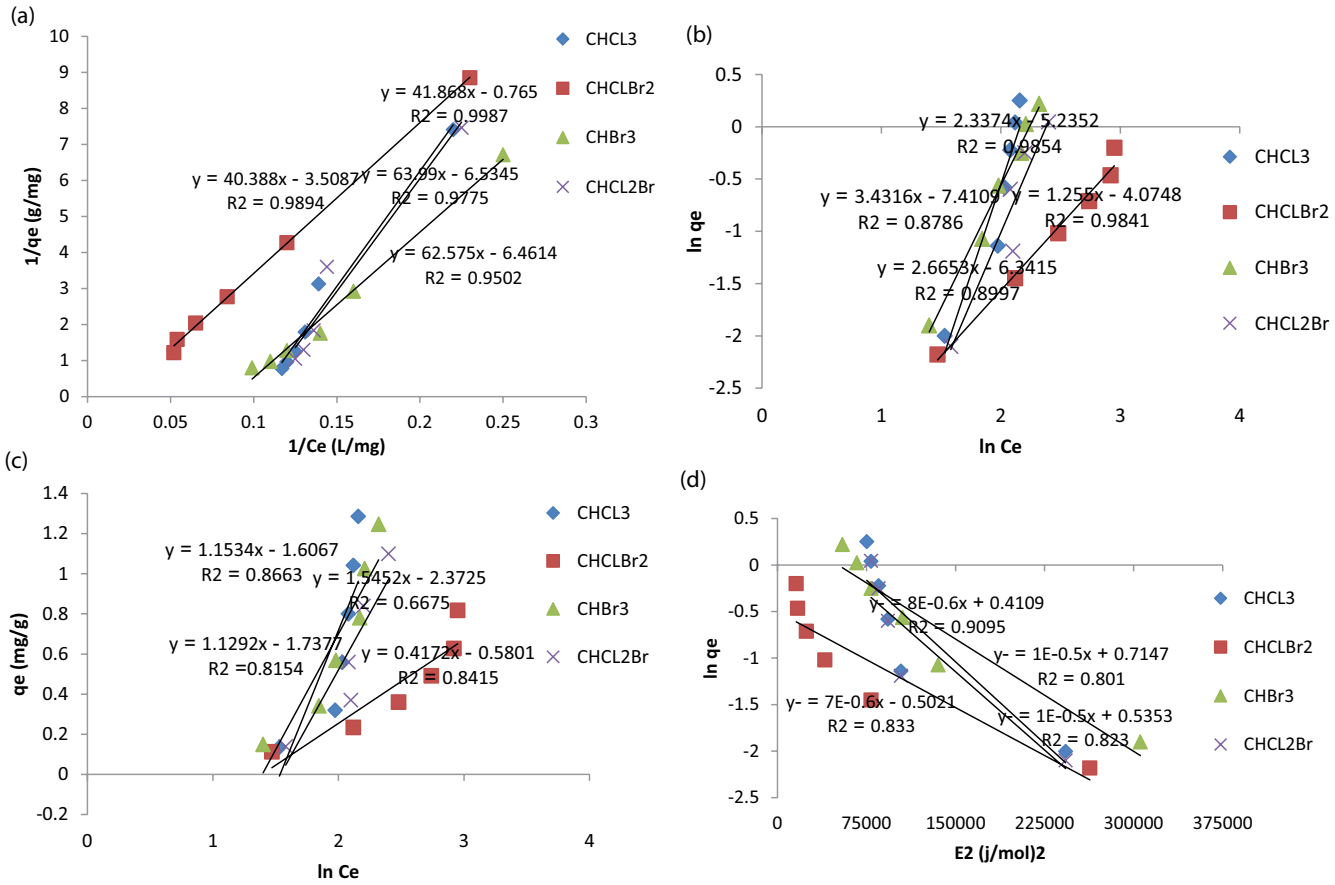

Fig. 12. (a) Langmuir isotherm, (b) Freundlich isotherm, (c) Temkin isotherm, and (d) Dubinin–Radushkevich isotherm for the adsorption of THMs (THMs conc = 30 mg L^{-1}, pH = 7.0, adsorbent dose = 50 mg, contact time = 50 min, temperature = 25°C, and stirring speed = 180 rpm).

adsorption is characterized by a uniform distribution of the binding energies up to some top binding energy [41]. The following introduces the linear form of the Temkin isotherm:

$$\log\left(\frac{1}{q_e}\right)=\log\left(\frac{K_L+1}{K_L q_m}\right)+\frac{1}{n}\log\frac{1}{C_e} \tag{6}$$

The plots of $\ln C_e$ vs. q_e for $CHCl_3$, $CHCl_2Br$, $CHClBr_2$, and $CHBr_3$ are displayed in Fig. 12c, and in Table 3, the summary of the linear isotherm parameters b_T, K_T, and the correlation coefficient are displayed. The b_T constant related to heat of sorption for $CHCl_3$, $CHCl_2Br$, $CHClBr_2$, and $CHBr_3$ onto *M. germanica* modified by $Fe_2(MoO_4)_3$ nanocomposite.

- To analyze the nature of adsorption, Dubinin–Radushkevich (D–R) isotherm model is utilized. In the ensuing equation, the linear form of this model is introduced:

$$\ln q_e=\ln q_m-\beta\varepsilon^2 \tag{7}$$

β in the foregoing formula stands for the activity coefficient relative to mean sorption energy ($mol^2\ kJ^{-2}$), and ε refers to the Polanyi potential which is calculable by the following equation:

$$\varepsilon=RT\ln\left(1+\frac{1}{C_e}\right) \tag{8}$$

In the foregoing formula, R stands for the ideal gas constant (8.3145 J mol K^{-1}) and T for absolute temperature (K) (Fig. 12d). E_a refers to the free energy change of adsorption (kJ mol^{-1}) which stands in need of transferring 1 mol of ions from solution to the adsorbent surface and is calculable by the ensuing equation [42]:

$$E_a=\frac{1}{\left(-2\beta\right)^{1/2}} \tag{9}$$

In this model, the mechanism of adsorption is considered physical if E_a is smaller than 8 kJ mol^{-1} but if E_a is greater than 20 kJ mol^{-1}, the mechanism of adsorption is considered to be chemical and finally if $8 > E_a < 20$ kJ mol^{-1}, the dominancy of chemical ion exchange in the adsorption is confirmed [43]. The E values –247.5, –256.3, –264.3, and –221.42 for $CHCl_3$, $CHCl_2Br$, $CHClBr_2$, and $CHBr_3$,

Table 3
Varied isotherm constants and correlation coefficients computed for the adsorption of $CHCl_3$, $CHCl_2Br$, $CHClBr_2$, and $CHBr_3$ onto *Mespilus germanica* modified by $Fe_2(MoO_4)_3$ nanocomposite

Isotherm	Equation	Parameters	Value of parameters for $CHCl_3$	Value of parameters for $CHCl_2Br$	Value of parameters for $CHClBr_2$	Value of parameters for $CHBr_3$
Langmuir	$q_e = q_m bC_e/(1 + bC_e)$	Q_m (mg g^{-1})	28.5	15.31	13.16	4.27
		K_L (L mg^{-1})	0.9	0.102	0.18	0.23
		R^2	0.9987	0.9894	0.9775	0.9502
Freundlich	$\ln q_e = \ln K_F + (1/n) \ln C_e$	n	0.42	0.3	0.28	0.16
		K_F (mg)$^{1-n}$ L^n g^{-1}	2.05	1.59	1.7	1.2
		R^2	0.9854	0.9841	0.8997	0.8786
Temkin	$\log\left(\frac{1}{q_e}\right) = \log\left(\frac{K_L+1}{K_L q_m}\right) + \frac{1}{n}\log\frac{1}{C_e}$	A_T (L mg^{-1})	4.03	4.64	4.723	4.938
		B_T	115.34	154.52	215.9	257.8
		R^2	0.8663	0.8415	0.8154	0.6675
Dubinin–Radushkevich (DR)	$\ln q_e = \ln Q_d - B\varepsilon^2$	Q_m (mg g^{-1})	15.9	10.5	6.5	2.07
		E (kJ mol^{-1})	–247.5	–256.3	–264.3	–221.42
		R^2	0.9095	0.833	0.823	0.801

respectively. This indicates that THMs adsorption onto *M. germanica* modified by $Fe_2(MoO_4)_3$ nanocomposite adsorbent is physical.

3.13. Analysis of the adsorption kinetic

In an aqueous medium, adsorption of a solute by a solid is performed via complex stages [44]. Numerous parameters relative to the state of the solid (generally with a very non-uniform reactive surface) and physico-chemical conditions under which the adsorption is taking place can affect the adsorption. Four kinetic models of (1) pseudo-first-order, (2) pseudo-second-order, (3) intra-particle diffusion model, and (4) Elovich were applied to the data to evaluate the adsorption kinetics of metals [45]. The adsorption kinetic data were described by the Lagergren pseudo-first-order model [46]. The following formula introduces the Lagergren:

$$\frac{dq_t}{dt} = K_1\left(q_e - q_t\right) \tag{10}$$

- Pseudo-first-order model is introduced through the ensuing equation:

$$\ln\left(q_e - q_t\right) = \ln q_e - K_1 t \tag{11}$$

where K_1 is the rate constant of adsorption (min^{-1}). The quantities of THMs adsorbed per unit mass of the adsorbent (mg g^{-1}) at equilibrium and time t are shown by q_e and q_t, respectively. q_e and q_t are calculable by the followings:

$$q_e = \frac{\left(C_i - C_e\right)V}{m} \tag{12}$$

$$q_t = \frac{\left(C_i - C_t\right)V}{m} \tag{13}$$

where C_t (mg L^{-1}) refers to the THMs concentrations at time t.

- The following equation expresses the pseudo-second-order model:

$$\frac{t}{q_t} = \frac{1}{k_2 q_e^2} + \frac{t}{q_e} \tag{14}$$

That K_{ad} stands for the rate constant of equation (g mg^{-1} min^{-1}) which is calculable from the plots of t/q_t vs. t. Also, $h = k_2 q_e^2$ (mg g^{-1} min^{-1}) (Fig. 13b).

- Elovich equation is expressed as:

$$q_t = \frac{1}{\beta}\ln\left(\alpha\beta\right) + \frac{1}{\beta}\ln t \tag{15}$$

where β shows the desorption constant (mg g^{-1} min^{-1}).

- The ensuing formula introduces the intra-particle diffusion model (Fig. 13):

$$q_t = k_{dif} t^{1/2} + C \tag{16}$$

where k_{intra} refers to the intra-particle diffusion rate constant (mg g^{-1} min$^{-1/2}$); k_{intra} is calculable from the slope between q_t vs. $t^{1/2}$; C is a constant.

The kinetic model with a greater correlation coefficient R^2 was considered and chosen as the most appropriate model. For evaluating the sorption performance of sorbents, k_d must be determined. The calculation of the distribution coefficient (k_d) of metal ions was carried out using the ensuing equation:

$$k_d = \left[\frac{C_i - C_e}{C_e}\right]\left(\frac{V}{m}\right) \tag{17}$$

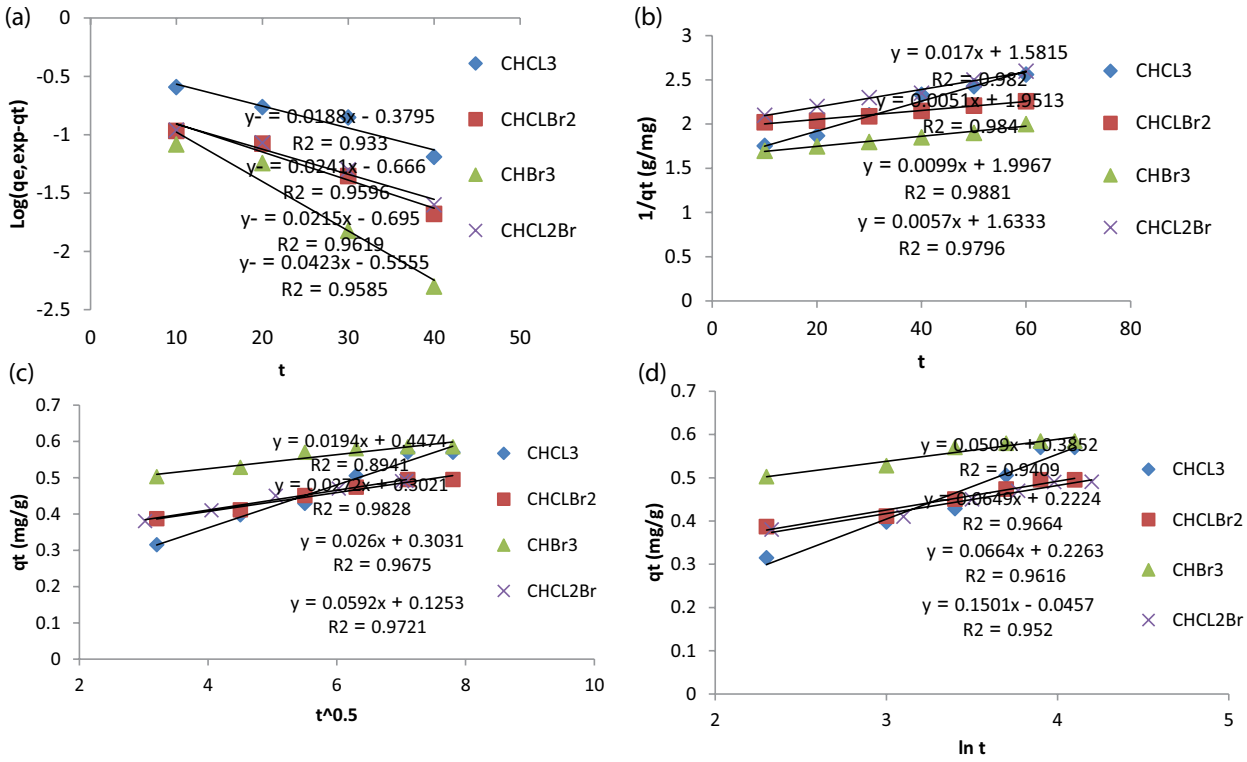

Fig. 13. (a) Pseudo-first-order, (b) pseudo-second-order, (c) Elovich, and (d) intra-particle diffusion model for THMs adsorption (THMs conc = 30 mg L^{-1}, pH = 7.0, adsorbent dose = 50 mg, contact time = 50 min, temperature = 25°C, and stirring speed = 180 rpm).

where V in the above-mentioned equation shows the solution volume (mL). Higher k_d value is a good indication for being a suitable and successful sorbent in eliminating metals.

In Table 4, the estimated correlation coefficient (R^2) values of the four kinetic models and other relative kinetic parameters are listed. The appropriateness of the pseudo-second-order kinetic model has been confirmed on the ground of the obtained values of the correlation coefficient (R^2). The pseudo-second-order kinetic model in comparison with other models revealed the highest conformity with the experimental data in explaining the adsorption mechanism of $CHCl_3$, $CHCl_2Br$, $CHClBr_2$, and $CHBr_3$ onto *M. germanica* modified by $Fe_2(MoO_4)_3$ nanocomposite (Fig. 13).

3.14. Adsorption thermodynamics

For the adsorption processes, 3 thermodynamic parameters of (1) Gibbs free energy change (ΔG°), (2) enthalpy change (ΔH°), and (3) entropy change ΔS° are considered. Their calculation is possible using the ensuing equations [47]:

$$\Delta G^\circ = -RT \ln K_{ad} \tag{18}$$

$$\ln K_{ad} \frac{\Delta H^\circ}{RT} + \frac{\Delta S^\circ}{R} \tag{19}$$

From a plot of lnK_e against 1/T, a graph (Fig. 14) is provided. By considering the slope of this graph, ΔG° can be acquired. A table containing a synopsis of the results of the thermodynamic parameter for the adsorption of $CHCl_3$, $CHCl_2Br$, $CHClBr_2$, and $CHBr_3$ onto developed *M. germanica* modified by $Fe_2(MoO_4)_3$ at diverse temperatures is provided (Table 5).

The estimation of ΔG° values became possible via applying the equation adsorption of THMs. As evident in Fig. 14, with an increase in the temperature from 298 to 348 K, a steep reduction in the *M. germanica* modified by $Fe_2(MoO_4)_3$ adsorbent was observed which proves the exothermicity nature of the process. Through utilizing the plots, the values of the thermodynamic parameters (Table 5), were calculated. Moreover, the negative value of GU supports the feasibility and spontaneity nature of the process. Secondly, the negative value of ΔH° strongly affirms the exothermicity nature of the adsorption and the value of ΔS° affirms an alteration in the randomness at the derived *M. germanica* modified by $Fe_2(MoO_4)_3$ solution interface within the sorption. The conformity of ΔG° values up to –4.7 kJ mol^{-1} for all $CHCl_3$, $CHCl_2Br$, $CHClBr_2$, and $CHBr_3$ with those of electrostatic interaction between sorption sites and the $CHCl_3$, $CHCl_2Br$, $CHClBr_2$, and $CHBr_3$ (physical adsorption) has been recorded. In this current article, the predominance of the physical adsorption mechanism in the sorption process has been confirmed by the obtained ΔG° values for THMs (<–5 kJ mol^{-1})[48].

3.15. Desorption

Close scrutiny of desorption is beneficial in exploring the possibility of recycling the adsorbents. Desorption of THMs by HCl is exhibited in Fig. 15. A range from 0.0125 to 0.2 M concentrations of HCl solutions was put to the test for eliminating THMs from the adsorbent. Based on

Table 4
Juxtaposition of the kinetic parameters for the elimination of $CHCl_3$, $CHCl_2Br$, $CHClBr_2$, and $CHBr_3$ by *Mespilus germanica* modified by $Fe_2(MoO_4)_3$ nanocomposite

Model	Parameters	Value of parameters for $CHCl_3$	Value of parameters for $CHCl_2Br$	Value of parameters for $CHClBr_2$	Value of parameters for $CHBr_3$
Pseudo-first-order kinetic: $\log(q_e - q_t) = \log(q_e) - \left(\frac{K_1}{2.303}\right)t$	$q_{e,cal}$ (mg g^{-1})	42.2	28.2	21.4	8.39
	K_1 (min^{-1})	0.04	0.1	0.06	0.0921
	R^2	0.933	0.9596	0.9585	0.9619
Pseudo-second-order kinetic: $\frac{t}{q_t} = \frac{1}{K_2 q_e^2} + \left(\frac{1}{q_e}\right)t$	q (mg g^{-1})	70.922	61	54	12.8
	K_2 (g mg min^{-1})	9.2	6.724	3.5	0.21
	R^2	0.9820	0.9840	0.9881	0.9796
Intra-particle diffusion: $q_t = k_{intra}(t)^{1/2} + c$	K_i ((mg g^{-1}) $min^{-0.5}$)	5.9163	2.5988	1.937	1.0339
	C (Å)	12.53	30.304	44.736	72.84
	R^2	0.952	0.9409	0.9616	0.9664
Elovich: $q_t = \frac{1}{\beta}\ln(\alpha\beta) + \frac{1}{\beta}\ln(t)$	α (g mg min^{-1})	20.4	9,817.42	367.44	4.18
	β (g mg^{-1})	0.07	0.196	0.17	–700.0
	R^2	0.9721	0.9675	0.9828	0.8941

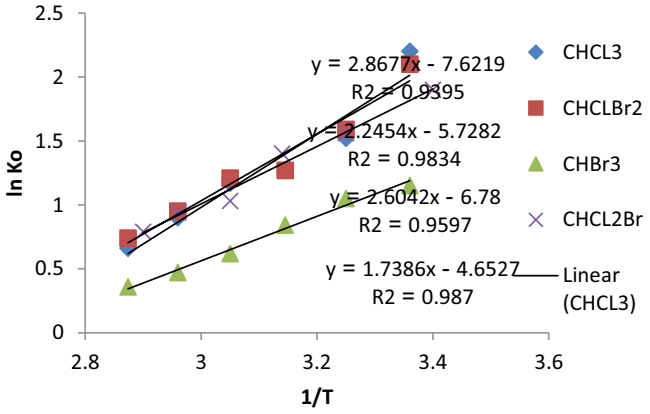

Fig. 14. Plot of $\ln K_c$ vs. $1/T$ for the estimation of thermodynamic parameters (THMs conc = 30 mg L^{-1}, pH = 7.0, adsorbent dose = 50 mg, contact time = 50 min, temperature = 25°C, and stirring speed = 180 rpm).

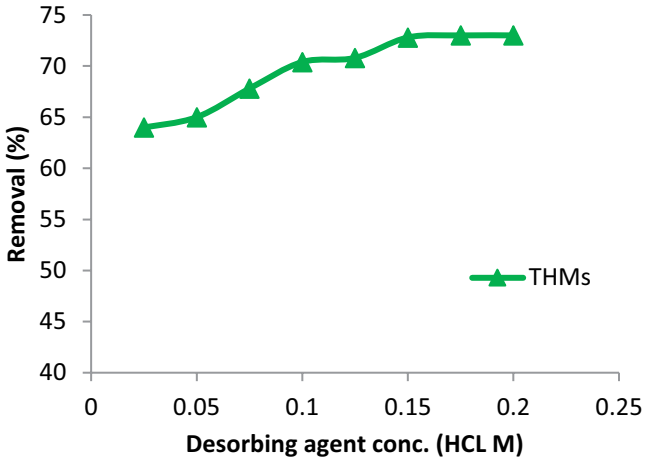

Fig. 15. Desorption plot of the THMs by HCl (desorbing agent volume = 50 mL, THMs conc = 30 mg L^{-1}, adsorbent dose = 50 mg, contact time = 60 min, temperature = 25°C, and stirring speed = 180 rpm).

the obtained results, it becomes evident that the maximum desorption of THMs was 72.19% from *M. germanica* modified by $Fe_2(MoO_4)_3$ nanocomposite, by HCl (0.15 M). Thenceforth, no competition for exchange sites was observed between THMs and H^+ ions and consequently THMs were released into the solution.

4. Conclusions

In the present article, a comprehensive study of *M. germanica* modified by $Fe_2(MoO_4)_3$ nanocomposite proved its applicability as an available, powerful, and inexpensive adsorbent for the elimination of THMs from aqueous media. The optimum values of the pH, adsorbent dosage, THMs concentration, and contact time were found to be 7, 50 mg, 30 mg L^{-1}, and 50 min for $CHCl_3$, $CHCl_2Br$, $CHClBr_2$, and $CHBr_3$, respectively. Studying the impact of various process parameters revealed that when THMs concentration increased, percent adsorption decreased but the percentage adsorption rose when the adsorbent dosage rose. Therefore, the adsorbent has excellent adsorption properties for THMs, even though the solution had a low concentration of THMs. It is also noted that the small molecules radius, $CHCl_3$ is the most preferentially adsorbed onto *M. germanica* modified by $Fe_2(MoO_4)_3$ nanocomposite, followed by $CHCl_2Br$, $CHClBr_2$, and $CHBr_3$. This may be attributed to the fact that adsorption occurs with molecules that are small enough in size enter the inner cavities and

Table 5
Thermodynamic parameters for the adsorption of $CHCl_3$, $CHCl_2Br$, $CHClBr_2$, and $CHBr_3$ onto *Mespilus germanica* modified by $Fe_2(MoO_4)_3$ adsorbent

THMs (mg L^{-1})	T (K)	K_c	Value of $\Delta S°$ (J mol K^{-1})	Value of $\Delta H°$ (kJ mol^{-1})	Value of $\Delta G°$ (kJ mol^{-1})
$CHCl_3$	298	8.62	–63.4	–23.84	–5.337
	308	4.56			–3.885
	318	3.57			–3.365
	328	3.2			–3.172
	338	2.39			–2.448
	348	1.98			–1.976
$CHCl_2Br$	298	8.09	–56.4	–21.65	–5.18
	308	4.88			–4.06
	318	3.55			–3.35
	328	3.27			–3.24
	338	2.57			–2.653
	348	2.13			–2.188
$CHClBr_2$	298	4.38	–40.95	–16.12	–3.66
	308	4.38			–3.78
	318	3.76			–3.5
	328	3.17			–3.15
	338	2.13			–2.12
	348	1.7			–1.54
$CHBr_3$	298	3.17	–38.683	–14.455	–2.858
	308	2.76			–2.6
	318	2.33			–2.236
	328	1.87			–1.706
	338	1.62			–1.356
	348	1.43			–1.035

diffuse through the pores with the least steric hindrance, especially in the micropore region for these small molecules. The maximum elimination of THMs by the adsorbent was observed at pH 7.0. The maximum adsorption capacities (q_{max}) were found to be 28.5, 15.3, 13.15, and 4.27 mg g^{-1} for $CHCl_3$, $CHCl_2Br$, $CHClBr_2$, and $CHBr_3$, respectively. Equilibrium adsorption showed the system followed both Langmuir and Freundlich models. The adsorption mechanism for these adsorbents was considered to be physical which was confirmed by the E_a obtained from Dubinin–Radushkevich isotherm. The thermodynamic parameters such as free energy ($\Delta G°$), enthalpy ($\Delta H°$), and entropy ($\Delta S°$) of adsorption. The negative value of ($\Delta G°$, $\Delta H°$, and $\Delta S°$) confirmed the sorption process was exothermic reflects the affinity of *M. germanica* modified by $Fe_2(MoO_4)_3$ nanocomposite for removing $CHCl_3$, $CHCl_2Br$, $CHClBr_2$, and $CHBr_3$ onto *M. germanica* modified by $Fe_2(MoO_4)_3$ nanocomposite process requires heat. The kinetics analysis came to this conclusion that THMs elimination followed the pseudo-second-order rate equation. Furthermore, the likelihood of recycling the adsorbent was expressed by desorption studies. The obtained outcomes from the nonlinear regression-based analysis supported this fact that the derived empirical models could provide an up to par prediction of performance for $CHCl_3$, $CHCl_2Br$, $CHClBr_2$, and $CHBr_3$ with very high determination coefficients (R^2 = 0.994–0.984). Finally, the statistical results with 88% certainty undoubtedly corroborated that the recommended equations could successfully be applied for the adsorption of THMs from aqueous media. Further investigations on the applicability of this adsorbent for the elimination of other material are highly recommended. Scrutinizing the possible industrial application of this material is also recommended. The obtained results in this work proved the suitability of the present process for the effective elimination of pollutants from aqueous media.

Acknowledgments

The authors gratefully acknowledge partial support of this work by the Islamic Azad University, Branch of Omidiyeh Iran.

References

[1] H. Chiu, S.S. Tsai, T.N. Wu, C.Y. Yang, Effect modification of the association between trihalomethanes and pancreatic cancer by drinking water hardness: evidence from an ecological study, J. Environ. Res., 110 (2010) 513-518.
[2] G. Hasani, A. Maleki, H. Daraei, R. Ghanbari, M. Safari, G. McKay, K. Yetilmezsoye, F. Ilhane, N. Marzban,

A comparative optimization and performance analysis of four different electrocoagulation–flotation processes for humic acid removal from aqueous solutions, J. Process Saf. Environ. Prot., 121 (2019) 103–117.
[3] K. Babi, K.M. Koumenides, A.D. Nikolaou, C.A. Makri, F.K. Tzoumerkas, T.D. Lekkas, Pilot study of the removal of THMs, HAAs and DOC from drinking water by GAC adsorption, Desalination, 210 (2007) 215–224.
[4] E. Niknam, A.A. Babaei, A. Ansari, Removal of trihalomethane precursors from water using activated carbon obtained from oak wood residue: kinetic and isotherm investigation of adsorption process, Desal. Water Treat., 92 (2017) 116–127.
[5] J. Hernandez Bourdon, F.M. Linares, Trihalomethanes in comerio drinking water and their reduction by nanostructured materials, Soft Nanosci. Lett., 4 (2014) 31–41.
[6] A.H.H. Daifullah, M.A. Rizk, H.M. Aly, S.M. Yakout, M. Refaat Hassen, Treatment of some organic pollutants (THMs) using activated carbon derived from local agro-residues, Appl. Sci. Res., 2 (2011) 357–370.
[7] B. Brian Bolto, D. Dixon, Removal of THM precursors by coagulation or ion exchange, Water Res., 36 (2002) 5066–5073.
[8] C. Lu, Y.L. Chung, Adsorption of trihalomethanes from water with carbon nano tubes, Water Res., 39 (2005) 1183–1189.
[9] R.S. Pirkle, J.D. Jack, P.A. Bukaveckas, Reduction in trihalomethane formation potential through air oxidation, J. Environ. Inf. Arch., 4 (2006) 273–279.
[10] V. Uyak, I. Koyuncu, I. Oktem, M. Cakmakci, I. Toroz, Removal of trihalomethanes from drinking water by nanofiltration membranes, J. Hazard. Mater., 152 (2008) 789–794.
[11] K. Ozdemir, O. Gungor, Development of statistical models for trihalomethane (THMs) removal in drinking water sources using carbon nanotubes (CNTs), Water Air Soil, 44 (2018) 680–690.
[12] S.M. Yakout, Removal of trihalomethanes from aqueous solution through adsorption and photodegradation, Adsorpt. Sci. Technol., 28 (2010) 601–610.
[13] N. Fischer, A. Ghosh, B. Talabi, C. Seide, P. Westerhoff, Chlorine addition prior to granular activated carbon contactors improves trihalomethane control, Water Sci. J., 10 (2018) 1–10.
[14] G.D.C. Cunha, L. Romao, M. Santos, B. Araujo, S. Navickiene, V. De Padua, Adsorption of trihalomethanes by humin: batch and fixed bed column studies, J. Bioresour. Technol., 101 (2010) 3345–3354.
[15] S. Rasheed, L.C. Campos, J.K. Kim, Q. Zhou, I. Hashmi, Optimization of total trihalomethanes (TTHMs) and their precursors removal by granulated activated carbon (GAC) and sand dual media by response surface methodology (RSM), J. Water Sci. Technol., 16 (2016) 783–793.
[16] K. Ozdemir, Characterization of natural organic matter in conventional water treatment processes and evaluation of THMs formation with chlorine, Sci. World J., 23 (2014) 201–207.
[17] P. Roccaro, F.G.A. Vagliasindi, G.V. Korshin, Relationships between trihalomethanes, haloacetic acids, and haloacetonitriles formed by the chlorination of raw, treated, and fractionated surface waters, J. Water Supply Res. Technol., 63 (2014) 21–30.
[18] P. Kralik, H. Kusic, N. Koprivanac, A.L. Bozic, Degradation of chlorinated hydrocarbons by UV/H_2O_2: the application of experimental design and kinetic modeling approach, Chem. Eng. J., 158 (2010) 154–166.
[19] K. Irfana Moideen, A.M. Isloor, A.F. Ismail, A. Obaid, H.-K. Fun Fabrication and characterization of new PSF/PPSUUF blend membrane for heavy metal rejection, Desal. Water Treat., 52 (2015) 1–10.
[20] A.O. Salawudeen, B.S. Tawabini, T.A. Saleh, A.M. Al-Shaibani, Evaluation of the removal of phenol from contaminated water by graphene oxide functionalized with poly diallydimethyl ammonium chloride (GPDADMAC), Desal. Water Treat., 162 (2019) 341–352.
[21] G.H. Vatankhah, T. Ershad, Enhanced removal of trihalomethanes (THMs) from aqueous solutions using activated carbon from Walnut wood (WC) on equilibrium, thermodynamic and kinetics, J. Phys. Theor. Chem., 15 (2018) 1–14.
[22] A.A. Basaleh, M.H. Al-Malack, T.A. Saleh, Metal removal using chemically modified eggshells: preparation, characterization, and statistical analysis, Desal. Water Treat., 173 (2020) 313–330.
[23] J.F. Davidson, D. Harrison, Fluidized Particles, Cambridge University Press, New York, NY, 1963.
[24] A. Zhang, W. Chen, Z. Gu, Q. Li, G. Shi, Mechanism of adsorption of humic acid by modified aged refuse, RSC Adv., 8 (2018) 33642–33651.
[25] P. Senthil Kumar, S. Ramalingam, C. Senthamarai, P. Vijayalakshmi, S. Sivanesan, Adsorption of dye from aqueous solution by cashew nut shell: studies on equilibrium isotherm, kinetics and thermodynamics of interactions, Desalination, 261 (2010) 52–60.
[26] T.A. Saleh, Mercury sorption by silica/carbon nanotubes and silica/activated carbon: a comparison study, J. Water. Supply Res. Technol., 64 (2015) 892–903.
[27] Y.H. Chen, C.S. Yeh, A new approach for the formation of alloy nanoparticles: laser synthesis of gold–silver alloy from gold–silver colloidal mixtures electronic supplementary information (ESI) available: experimental details, UV-VIS spectra, TEM images and EDX analysis for molar ratios (Au:Ag) of 1:2 and 2:1. See http://www.rsc.org/suppdata/cc/b0/b009854j/, Chem. Commun., 4 (2001) 371–372.
[28] T.A. Saleh, Naeemullah, M. Tuzen, A. Sarı, Polyethylenimine modified activated carbon as novel magnetic adsorbent for the removal of uranium from aqueous solution, Chem. Eng. Res. Des., 117 (2017) 218–227.
[29] K. Nath, S. Panchani, M.S. Bhakhar, S. Chatrola, Preparation of activated carbon from dried pods of *Prosopis cineraria* with zinc chloride activation for the removal of phenol, J. Environ. Sci. Pollut. Res., 20 (2013) 4030–4045.
[30] C. Byram, V.R. Soma, 2,4-dinitrotoluene detected using portable Raman spectrometer and femtosecond laser fabricated Au–Ag nanoparticles and nanostructures, Nanostruct. Nano-objects, 12 (2017) 121–129.
[31] M.H. Dehghani, M. Mohammadi, M.A. Mohammadi, A.H. Mahvi, K. Yetilmezsoy, A. Bhatnagar, B. Heibati, G. McKay, Equilibrium and kinetic studies of trihalomethanes adsorption onto multi-walled carbon nanotubes, Water Air Soil Pollut., 227 (2016) 332–344.
[32] M.T. Samadi, S. Nasseri, A.R. Mesdaghinia, Removal of chloroform ($CHCl_3$) from Tehran drinking water by GAC and air stripping columns, Iran. J. Environ. Health Sci. Eng., 1 (2004) 5–12.
[33] M. Masoudzadeh, N. Karachi, Enhanced removal of humic acids (HAs) from aqueous solutions using MWCNTs modified by N-(3-nitro-benzylidene)-N-trimethoxysilylpropyl-ethane-1,2-diamine on equilibrium, thermodynamic and kinetics, J. Phys. Theor. Chem., 14 (2018) 259–270.
[34] A.A. Babaei, L. Atari, M. Ahmadi, K. Ahmadiangali, M. Zamanzadeh, N. Alavi, Trihalomethanes formation in Iranian water supply systems: predicting and modeling, J. Water Health, 13 (2015) 859–869.
[35] A. Naghizadeh, S. Nasseri, S.H. Nazmara, Removal of trichloroethylene from water by adsorption onto multi wall carbon nanotubes, Iran. J. Environ. Health. Sci. Eng., 8 (2011) 317–324.
[36] G. Asgari, B. Roshani, G. Ghanizadeh, The investigation of kinetic and isotherm of fluoride adsorption onto functionalize pumice stone, J. Hazard. Mater., 217–218 (2012) 123–132.
[37] T.A. Saleh, M. Tuzen, A. Sari, Polyamide magnetic palygorskite for the simultaneous removal of Hg(II) and methyl mercury; with factorial design analysis, J. Environ. Manage., 211 (2018) 323–333.
[38] B. Heibati, M. Ghoochani, A.B. Albadarin, A. Mesdaghinia, A.S.H. Makhlouf, M. Asif, A. Maity, I. Tyagi, S. Agarwal, V.K. Gupta, Removal of linear alkyl benzene sulfonate from aqueous solutions by functionalized multi-walled carbon nanotubes, J. Mol. Liq., 213 (2016) 339–344.
[39] I. Langmuir, The adsorption of gases on plane surfaces of glass, mica and platinum, J. Am. Chem. Soc., 40 (1918) 1361–1403.
[40] H.M.F. Freundlich, Over the adsorption in solution, J. Phys. Chem., 57 (1906) 385–470.

[41] M. Temkin, V. Levich, Adsorption equilibrium on heterogeneous surface, Zh. Fiz. Kim, 20 (1946) 1441–1457.
[42] N.D. Hutson, R.T. Yang, Theoretical basis for the Dubinin-Radushkevitch (D-R) adsorption isotherm equation, Adsorption, 3 (1997) 189–195.
[43] M.M. Dubinin, Modern state of the theory of volume filling of micropore adsorbents during adsorption of gases and steams on carbon adsorbent, Zh. Fiz. Khim., 39 (1965) 1305–1317.
[44] T.A. Saleh, Isotherm, kinetic, and thermodynamic studies on Hg(II) adsorption from aqueous solution by silica-multiwall carbon nanotubes, J. Environ. Sci. Pollut. Res., 22 (2015) 16721–16731.
[45] Y.S. Ho, Kinetics and thermodynamics of lead ion sorption on palm kernel fibre from aqueous solution, Process Biochem., 40 (2005) 3455–3461.
[46] T.A. Saleh, Simultaneous adsorptive desulfurization of diesel fuel over bimetallic nanoparticles loaded on activated carbon, J. Cleaner Prod., 172 (2018) 2123–2132.
[47] M.A. Mohammed, A.H. Hassan, M.A. EL-Messiry, R.A. Hazzaa, Removal of trihalomethanes by dual filtering media (GAC-Sand) at El-Manshia water purification plant, J. Egypt. Public Health Assoc., 81 (2006) 241–258.
[48] M. Ebrahimi, S. Bagheri, M. Maleki Taleghani, M. Ghorabani, Humic acids elimination from aqueous media utilizing derived activated carbon from raw maize tassel on equilibrium, thermodynamic and kinetics, Desal. Water Treat., 60 (2019) 1–8.